Characterizations of realized metal-insulator-silicon-insulator-metal waveguides and nanochannel fabrication via insulator removal

Min-Suk Kwon,[1,*] Jin-Soo Shin,[2] Sang-Yung Shin,[2] and Wan-Gyu Lee[3]

[1]*School of Electrical and Computer Engineering, Ulsan National Institute of Science and Technology, 50 UNIST-gil, Eonyang-eup, Ulju-gun, Ulsan 689-798, South Korea*
[2]*Department of Electrical Engineering, Korea Advanced Institute of Science and Technology, 291 Daehak-ro, Yuseong-gu, Daejeon 305-701, South Korea*
[3]*National Nano Fab Center, 291 Daehak-ro, Yuseong-gu, Daejeon 305-806, South Korea*
[*]*mskwon@unist.ac.kr*

Abstract: We investigate experimentally metal-insulator-silicon-insulator-metal (MISIM) waveguides that are fabricated by using fully standard CMOS technology. They are hybrid plasmonic waveguides, and they have a feature that their insulator is replaceable with functional material. We explain a fabrication process for them and discuss fabrication results based on 8-inch silicon-on-insulator wafers. We measured the propagation characteristics of the MISIM waveguides that were actually fabricated to be connected to Si photonic waveguides through symmetric and asymmetric couplers. When incident light from an optical source has transverse electric (TE) polarization and its wavelength is 1318 or 1554 nm, their propagation losses are between 0.2 and 0.3 dB/μm. Excess losses due to the symmetric couplers are around 0.5 dB, which are smaller than those due to the asymmetric couplers. Additional measurement results indicate that the MISIM waveguide supports a TE-polarized hybrid plasmonic mode. Finally, we explain a process of removing the insulator without affecting the remaining MISIM structure to fabricate ~30-nm-wide nanochannels which may be filled with functional material.

OCIS codes: (240.6680) Surface plasmons; (250.5403) Plasmonics; (130.2790) Guided waves.

References and links

1. M. L. Brongersma, J. A. Schuller, J. White, Y. C. Jun, S. I. Bozhevolnyi, T. Sondergaard, and R. Zia, "Nanoplasmonics: Components, Devices, and Circuits," in *Plasmonic Nanoguides and Circuits,* S. I. Bozhevolnyi, ed. (Pan Stanford Publishing Pte. Ltd., 2009).
2. M. L. Brongersma and V. M. Shalaev, "Applied physics. The case for plasmonics," Science **328**(5977), 440–441 (2010).
3. S. I. Bozhevolnyi, V. S. Volkov, E. Devaux, J.-Y. Laluet, and T. W. Ebbesen, "Channel plasmon subwavelength waveguide components including interferometers and ring resonators," Nature **440**(7083), 508–511 (2006).
4. C. L. C. Smith, B. Desiatov, I. Goykmann, I. Fernandez-Cuesta, U. Levy, and A. Kristensen, "Plasmonic V-groove waveguides with Bragg grating filters via nanoimprint lithography," Opt. Express **20**(5), 5696–5706 (2012).
5. D. Kalavrouziotis, S. Papaioannou, G. Giannoulis, D. Apostolopoulos, K. Hassan, L. Markey, J.-C. Weeber, A. Dereux, A. Kumar, S. I. Bozhevolnyi, M. Baus, M. Karl, T. Tekin, O. Tsilipakos, A. Pitilakis, E. E. Kriezis, H. Avramopoulos, K. Vyrsokinos, and N. Pleros, "0.48Tb/s (12x40Gb/s) WDM transmission and high-quality thermo-optic switching in dielectric loaded plasmonics," Opt. Express **20**(7), 7655–7662 (2012).
6. C. Garcia, V. Coello, Z. Han, I. P. Radko, and S. I. Bozhevolnyi, "Partial loss compensation in dielectric-loaded plasmonic waveguides at near infra-red wavelengths," Opt. Express **20**(7), 7771–7776 (2012).
7. Z. Han, A. Y. Elezzabi, and V. Van, "Experimental realization of subwavelength plasmonic slot waveguides on a silicon platform," Opt. Lett. **35**(4), 502–504 (2010).
8. R. Salas-Montiel, A. Apuzzo, C. Delacour, Z. Sedaghat, A. Bruyant, P. Grosse, A. Chelnokov, G. Lerondel, and S. Blaize, "Quantitative analysis and near-field observation of strong coupling between plasmonic nanogap and silicon waveguides," Appl. Phys. Lett. **100**(23), 231109 (2012).
9. M. Wu, Z. Han, and V. Van, "Conductor-gap-silicon plasmonic waveguides and passive components at subwavelength scale," Opt. Express **18**(11), 11728–11736 (2010).

#173002 - $15.00 USD Received 20 Jul 2012; revised 4 Sep 2012; accepted 4 Sep 2012; published 10 Sep 2012

10. I. Goykhman, B. Desiatov, and U. Levy, "Experimental demonstration of locally oxidized hybrid silicon-plasmonic waveguide," Appl. Phys. Lett. **97**(14), 141106 (2010).
11. J. A. Summers and R. J. Ram, "Thermal and optical characterization of resonant coupling between surface plasmon polariton and semiconductor waveguides," Appl. Phys. Lett. **99**(18), 181118 (2011).
12. V. J. Sorger, N. Pholchai, E. Cubukcu, R. F. Oulton, P. Kolchin, C. Borschel, M. Gnauck, C. Ronning, and X. Zhang, "Strongly enhanced molecular fluorescence inside a nanoscale waveguide gap," Nano Lett. **11**(11), 4907–4911 (2011).
13. M.-S. Kwon, "Metal-insulator-silicon-insulator-metal waveguides compatible with standard CMOS technology," Opt. Express **19**(9), 8379–8393 (2011).
14. S. Zhu, T. Y. Liow, G. Q. Lo, and D. L. Kwong, "Silicon-based horizontal nanoplasmonic slot waveguides for on-chip integration," Opt. Express **19**(9), 8888–8902 (2011).
15. S. Zhu, G. Q. Lo, and D. L. Kwong, "Nanoplasmonic power splitters based on the horizontal nanoplasmonic slot waveguide," Appl. Phys. Lett. **99**(3), 031112 (2011).
16. S. Zhu, G. Q. Lo, and D. L. Kwong, "Electro-absorption modulation in horizontal metal-insulator-silicon-insulator-metal nanoplasmonic slot waveguides," Appl. Phys. Lett. **99**(15), 151114 (2011).
17. Refractive Index Database, *http://refractiveindex.info*.
18. H. S. Lee, C. Awada, S. Boutami, F. Charra, L. Douillard, and R. E. de Lamaestre, "Loss mechanisms of surface plasmon polaritons propagating on a smooth polycrystalline Cu surface," Opt. Express **20**(8), 8974–8981 (2012).
19. J. Buhler, F.-P. Steiner, and H. Baltes, "Silicon dioxide sacrificial layer etching in surface micromachining," J. Micromech. Microeng. **7**(1), R1–R13 (1997).
20. A. Witvrouw, B. Du Bois, P. De Moor, A. Verbist, C. Van Hoof, H. Bender, and K. Baert, "A comparison between wet HF etching and vapor HF etching for sacrificial oxide removal," Proc. SPIE **4174**, 130–141 (2000).
21. C.-Y. Lin, X. Wang, S. Charkravarty, B. S. Lee, W. Lai, J. Luo, A. K.-Y. Jen, and R. T. Chen, "Electro-optic polymer infiltrated silicon photonic crystal slot waveguide modulator with 23 dB slow light enhancement," Appl. Phys. Lett. **97**(9), 093304 (2010).

1. Introduction

Nanoplasmonic waveguides are metal-based waveguides that support a surface-plasmon polariton (SPP) based mode whose dimensions are below the diffraction limit [1]. Nowadays there are increasing demands to merge electronic and photonic devices on a chip scale as a breakthrough to overcome the limit of electronic-only devices [2]. Since nanoplasmonic waveguide devices are expected to play a key role in satisfying such demands, diverse nanoplasmonic waveguides with different structures have been proposed, theoretically investigated, and realized in some cases [3–12]. A few examples are channel plasmon polariton waveguides [3, 4], dielectric-loaded surface plasmon polariton waveguides [5, 6], metal-insulator-metal waveguides [7, 8], and hybrid plasmonic waveguides [9–12]. The last ones are especially prominent since they have both a small mode area and a long propagation distance. Some nanoplasmonic waveguides have been realized by using focused ion beam milling or e-beam lithography. However, such processes are out of standard CMOS technology. For nanoplasmonic waveguides to be a true bridge between photonics and electronics, they should be realizable with standard CMOS technology. For this purpose, silicon-based hybrid plasmonic waveguides like metal-insulator-silicon-insulator-metal (MISIM) waveguides, which are based on standard CMOS technology, have been studied [13–16]. Zhu et al. have investigated theoretically and experimentally the MISIM waveguide whose insulator is irreplaceable since it is fully covered by metal [14–16]. In contrast, Kwon investigated theoretically the MISIM waveguide whose insulator is replaceable via etching and filling [13]. The capability to change the insulator is important since it makes the MISIM waveguides more functional. For example, the MISIM waveguide whose insulator is substituted for electro-optic (EO) polymer may be used to implement high-speed nanoplasmonic modulators or switches. In addition, the MISIM waveguide with nonlinear optical material replacing the insulator may be applied to efficient all-optical devices that are based on the nonlinear optical effects of both the replacing material and silicon. Moreover, the MISIM waveguide with gain material replacing the insulator may compensate for loss coming from other MISIM waveguides. Therefore, if the insulator of the MISIM waveguide is removed and the empty space made by the insulator removal is ready to be filled with any functional material, the MISIM waveguide can be a platform for functional nanoplasmonic devices.

In this paper, we report experimental investigation of the MISIM waveguides proposed by Kwon. We explain the fabrication process based on fully standard CMOS technology, and

#173002 - $15.00 USD Received 20 Jul 2012; revised 4 Sep 2012; accepted 4 Sep 2012; published 10 Sep 2012

show the fabricated MISIM waveguides. Then, we discuss the measured characteristics of the MISIM waveguides. The characteristics include the propagation losses of the MISIM waveguides for transverse electric (TE) polarization and excess losses arising from coupling the MISIM waveguides to silicon photonic waveguides via tapering. The dependence of the propagation characteristics either on polarization or on a wavelength is also discussed. To demonstrate the applicability of the MISIM waveguide as a platform for functional nanoplasmonic devices, we established a process of removing the insulator without damaging the metal. We explain it and show resultant nanochannels in the MISIM waveguide. Finally, concluding remarks are given.

2. Fabrication process and fabricated MISIM waveguides

The structure of the realized MISIM waveguide, which is slightly modified from the structure in [13], is schematically shown in Fig. 1(a). Its metal is copper, which is essential for electrical interconnection in current electronic chips; its insulator is silicon oxide (SiO_x) that is conformally deposited around its silicon line; its silicon line has width w_S and height h_S. Because of its fabrication process, the thickness of the side insulator, t_{Il} is slightly thinner than the thickness of the top insulator, t_{It}. In addition, on the silicon line, there are a SiO_x layer of thickness 50 nm and a silicon nitride (SiN_x) layer of thickness ~10 nm. Also, its substrate has a ridge of height h_r below the silicon line, and the top surface of the metal is at distance d_m from the top surface of the insulator. For TE-polarized light, a quite large portion of the power carried by its hybrid plasmonic waveguide mode is confined to the thin insulator layers between the metal and Si lines. This is confirmed from the intensity profile of the mode as shown in Fig. 1(b). The profile was calculated for w_S = 160 nm, h_S = 250 nm, t_{Il} = 30 nm, t_{It} = 40 nm, h_r = 70 nm, and d_m = 120 nm by using the finite element method (FEM). (For the FEM, we used FIMMWAVE from Photon Design.)

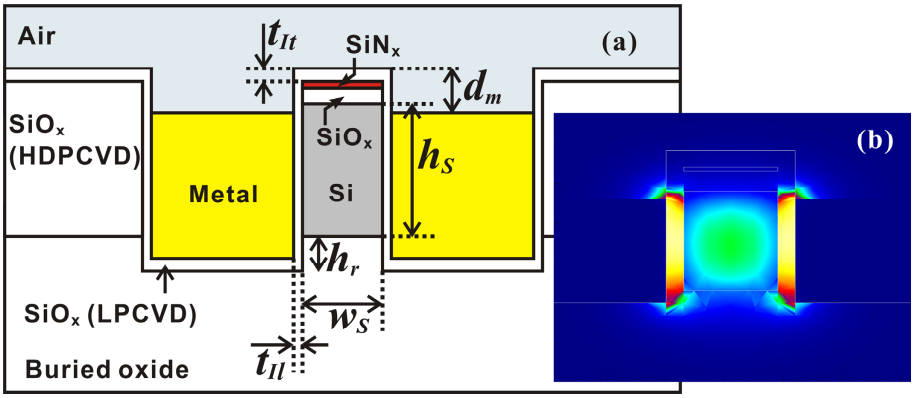

Fig. 1. (a) Cross-sectional structure of the realized MISIM waveguide. (b) Intensity profile of the MISIM waveguide mode which was calculated by using FIMMWAVE from Photon Design.

We fabricated the MISIM waveguides using an 8-inch silicon-on-insulator (SOI) wafer whose buried oxide is 2 μm thick and top silicon is 250 nm thick. The fabrication process started from low pressure chemical vapor deposition (LPCVD) of 50-nm-thick SiO_x and 100-nm-thick silicon nitride (SiN_x). The deposited SiN_x layer was used as an etch stop for the following chemical mechanical polishing (CMP). To make SiN_x–SiO_x–Si patterns, photoresist (PR) was coated on the wafer, and the PR was patterned by using KrF (248 nm) lithography. Different from the previous work in [14], a PR trimming process to reduce the dimensions of the patterned PR was not employed. This makes the fabrication process slightly simpler. With the patterned PR acting as an etching mask, the SiN_x, SiO_x, and Si layers were dry-etched. Over the SiN_x–SiO_x–Si patterns, ~800-nm-thick SiO_x was deposited. In this case, high-density plasma chemical vapor deposition (HDPCVD) was employed to minimize the protrusion of the deposited SiO_x surface due to the patterns. For further planarization of the surface, CMP

#173002 - $15.00 USD Received 20 Jul 2012; revised 4 Sep 2012; accepted 4 Sep 2012; published 10 Sep 2012

of the SiO_x surface was carried out until the surface of the SiN_x layer was reached. This CMP made the the SiN_x layer ~10 nm thick. To make a mold for the following Cu damascene process, another PR etching mask was formed by using the KrF lithography, and the unmasked SiO_x was dry-etched until the buried oxide below it was slightly removed to have the ridge. Then, LPCVD of SiO_x was carried out so that a thin SiO_x layer conformally covered the mold. Finally, ~800-nm-thick copper was deposited by sputtering, and CMP of the copper was done until the top surface of the thin SiO_x layer was exposed to form disconnected Cu lines filling troughs in the mold. During the CMP, the longer it is performed, the larger d_m is since SiO_x is so harder than copper that the former is less removed than the latter.

Figure 2(a) shows a photograph of the whole 8-inch wafer containing 85 chips each of which has dimensions of 20 mm × 15 mm. Every chip contains three groups of the MISIM waveguides. In the respective groups, w_S = ~160, ~190, and ~220 nm. These values are larger than those of the previous MISIM waveguides in [14] since the PR trimming process was not used. (As checked below, because of the larger values of w_S, the propagation characteristics of the MISIM waveguides are somewhat improved.) In every group, there are not only the MISIM waveguides but also reference waveguides that are Si photonic waveguides consisting of a Si line of width w_S, which is surrounded by the HDPCVD SiO_x. The left and right ends of the MISIM or reference waveguide of length l_M are connected to 450-nm-wide Si photonic waveguides of length $l_{S1}/2$ by increasing symmetrically the width of its Si line from w_S to 450 nm over a distance l_t, as shown in the top and middle of Fig. 2(b). The symmetrically tapered structure is hereafter called a symmetric coupler. For a set of the MISIM waveguides in the group for w_S = ~190 nm, their ends are connected to the 450-nm-wide Si photonic waveguides by increasing asymmetrically the width of their Si lines from w_S to 450 nm over a distance l_t, as shown in the bottom of Fig. 2(b). The asymmetrically tapered structure is hereafter called an asymmetric coupler. All the 450-nm-wide Si photonic waveguides are also connected to 5-μm-wide Si photonic waveguides of length $l_{S2}/2$, which reach the sides of a chip, through linear tapering over a distance of 200 μm [Fig. 2(b)]. For a set of the MISIM and reference waveguides in every group, l_M increases from 1 μm to 15 μm while l_t is set to 0.6 μm and l_{S2} + l_M is held at a constant. In the set, five MISIM waveguides and two reference waveguides have the same value of l_M. For another set of the MISIM waveguides in every group and for the set of the MISIM waveguides with the asymmetric couplers, l_t increases from 0.3 μm to 1.0 μm while l_M is set to 1 μm and l_{S2} + l_t is held at a constant. In the sets, three MISIM waveguides have the same value of l_t. For all the set, l_{S1} is set to 4 mm. Scanning electron microscope (SEM) images of the fabricated MISIM waveguides with the symmetric and asymmetric couplers are shown in Fig. 2(c) and 2(d), respectively. An SEM image of the cross-section of the MISIM waveguide is shown in Fig. 2(e). In the whole wafer, t_{Il} = ~30 nm, t_{It} = ~40 nm, h_r = ~70 nm, and d_m = ~120 nm, as checked from Fig. 2(e). At the place where the MISIM waveguide meets the 450-nm-wide Si photonic waveguide, there are unintended holes, which seem to have occurred during the Cu-CMP. The facets of the 5-μm-wide Si photonic waveguides were prepared by dicing and polishing the chips.

3. Measurement of the propagation characteristics of the MISIM waveguides

Light from a source was launched into the 5-μm-wide Si photonic waveguide by using lensed fiber spliced with polarization-maintaining fiber. Before light was incident on the polarization-maintaining fiber, its polarization was adjusted to be TE or transverse magnetic (TM) by using a polarization controller. Light from the 5-μm-wide Si photonic waveguide was coupled to another lensed fiber spliced with polarization-maintaining fiber, which was connected to an optical power meter. The wavelength λ of the source was either 1554 nm or 1318 nm. We measured the fiber-to-fiber insertion loss IL_{MS} (IL_{MA}) of the combinations of the waveguides in the top (bottom) of Fig. 2(b). We also measured the fiber-to-fiber insertion loss IL_R of the combinations of the waveguides in the middle of Fig. 2(b). For reference, the fiber-to-fiber insertion loss IL_{Si} of the combinations of the 5-μm-wide Si photonic waveguides and the 450-nm-wide Si photonic waveguide of length l_{S1}, which were co-fabricated on each chip, was measured. In the following parts, we discuss the results of the measurement.

#173002 - $15.00 USD Received 20 Jul 2012; revised 4 Sep 2012; accepted 4 Sep 2012; published 10 Sep 2012

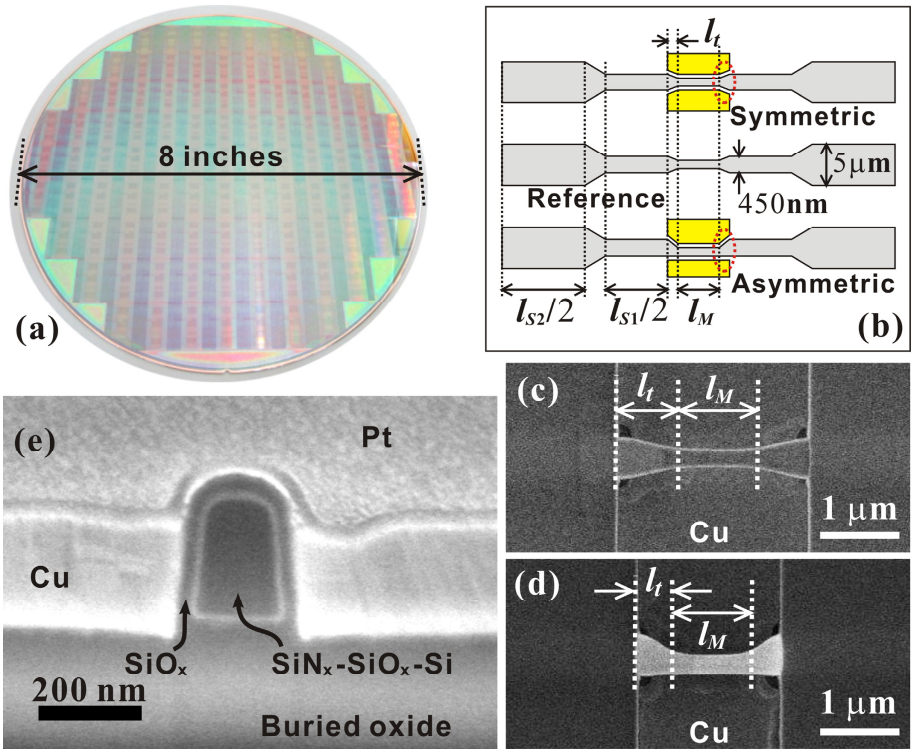

Fig. 2. (a) Photograph of the whole wafer. (b) Schematic diagrams of the fabricated combinations of the waveguides. The MISIM waveguide is connected to the 450-nm-wide Si photonic waveguides via the symmetric [top] or asymmetric [bottom] couplers. The reference waveguide is also connected to the 450-nm-wide Si photonic waveguides via the symmetric couplers [middle]. The 450-nm-wide Si photonic waveguides are connected to the 5-μm-wide Si waveguides. (c) SEM image of the MISIM waveguide with the symmetric couplers. (d) SEM image of the MISIM waveguide with the asymmetric couplers. (e) SEM image of the cross-section of the MISIM waveguide. Platinum over the MISIM waveguide was formed to prepare the cross-section by using focused ion beam.

3.1 Propagation loss for TE polarization

IL_{MS} and IL_R for TE polarization were measured with respect to l_M. Figures 3 and 4 show the relations of IL_{MS} and IL_R to l_M for the three values of w_S at the wavelengths of 1554 nm and 1318 nm, respectively. Not only in these figures but also in the following ones, the error bars correspond to the standard deviations of experimental data.

In Fig. 3(a), 3(c), and 3(e), as a first-order approximation, we fitted to the relation of IL_{MS} at λ = 1554 nm to l_M the straight line that is denoted as the red dotted line in the figures. The respective slopes of the straight lines correspond to the propagation losses of the MISIM waveguides with w_S = ~160, ~190, and ~220 nm. They are 0.262, 0.219, and 0.214 dB/μm, respectively. As w_S increases, the propagation loss decreases since a larger portion of the power of the MISIM waveguide mode becomes confined to the Si line. For comparison, the propagation constant β_M and attenuation coefficient α_M of the MISIM waveguide mode were calculated by using the FEM, and they are summarized in Table 1. Depending on how copper is prepared, the dielectric constant ε_{Cu} of copper changes, and so β_M and α_M change. If ε_{Cu} comes from a model based on Palik's handbook [17], the calculated values of α_M are much larger than the experimental values. However, if ε_{Cu} comes from the Drude model in [18], the former are smaller than the latter. The excess loss L_t caused by the symmetric coupler can be extracted from the intercept of the fitted straight line. The difference between the intercept and IL_{Si} for l_{S1} = 4 mm is equal to $2L_t$. The extracted values of L_t are 0.31 ± 0.17, 0.32 ± 0.17,

#173002 - $15.00 USD Received 20 Jul 2012; revised 4 Sep 2012; accepted 4 Sep 2012; published 10 Sep 2012

and 0.33 ± 0.17 dB, respectively, for w_S = ~160, ~190, and ~220 nm. Using the finite difference time domain (FDTD) method, we calculated L_t. (For the FDTD method, we used FDTD Solutions from Lumerical. The built-in model based on Palik's handbook was used for ε_{Cu}.) The calculated values of L_t are 0.623, 0.513, and 0.442 dB, respectively, and they are comparable to the experimental values. The experimental values α_M and L_t are smaller than those of the previous MISIM waveguides with w_S = ~134 nm and t_{Il} = ~12 nm in [14], which are 0.37 dB/μm and 0.42 dB.

As shown in Fig. 3(a), 3(c), and 3(e), the measured data deviate from the straight line. The deviation may arise from measurement errors and non-uniformity in the fabricated MISIM waveguides with the same length. However, it should be considered that the chip itself has the characteristics of Fabry-Perot resonance. Consequently, the linear fitting may not be adequate. An expression of IL_{MS} was derived from a simple model in which the Fabry-Perot resonance of the chip is considered, and it is

$$IL_{MS} = \frac{T_{S2}^2 T_t^2 \exp[-(\alpha_{S2} l_{S2} + \alpha_{S1} l_{S1} + \alpha_M l_M)]}{\left|1 - R_{S2} T_t^2 \exp[-j2(\beta_{S2} l_{S2} + \beta_{S1} l_{S1} + \beta_M l_M + \phi)] \exp[-(\alpha_{S2} l_{S2} + \alpha_{S1} l_{S1} + \alpha_M l_M)]\right|^2}. \quad (1)$$

In Eq. (1), T_{S2} and R_{S2} are the transmittance and the reflectance at the facets of the 5-μm-wide Si photonic waveguides; β_{S2} (β_{S1}) and α_{S2} (α_{S1}) are the propagation constant and the attenuation coefficient of the 5-μm-wide (450-nm-wide) Si photonic waveguides; T_t is the transmittance of the symmetric couplers; ϕ is a constant phase. We assumed that light is perfectly transferred between the 5-μm-wide Si photonic waveguide and the 450-nm-wide one and that there is no reflection due to the symmetric couplers. $l_{S2} + l_M$ was held at 6 mm. β_{S2} and β_{S1} were calculated by using the FEM; T_{S2} was calculated from overlap integral between a Gaussian beam from the lensed fiber and the fundamental mode of the 5-μm-wide Si photonic waveguide; R_{S2} was estimated from the Fresnel reflectivity given by $[\beta_{S2}/(2\pi/\lambda) - 1]^2 / [\beta_{S2}/(2\pi/\lambda) + 1]^2$. α_{S2} was estimated from the measured fiber-to-fiber insertion losses of the co-fabricated 5-μm-wide Si photonic waveguides; α_{S1} was extracted from the measured relation of IL_{Si} to l_{S1}; α_{S2} and α_{S1} are 0.19 and 0.63 dB/mm, respectively. Using this simple model, we calculated the relations of IL_{MS} to l_M, which are denoted as the blue solid lines in Fig. 3(a), 3(c), and 3(e). Adjusting the values of T_t, β_M, α_M, and ϕ, we fitted the calculated curve of IL_{MS} vs. l_M to the measured values of IL_{MS}. The resultant values of the fitting parameters are summarized in Table 2. The results of the fitting indicate that the somewhat scattered values of IL_{MS} are explained by the Fabry-Perot resonance character of the chip.

#173002 - $15.00 USD Received 20 Jul 2012; revised 4 Sep 2012; accepted 4 Sep 2012; published 10 Sep 2012

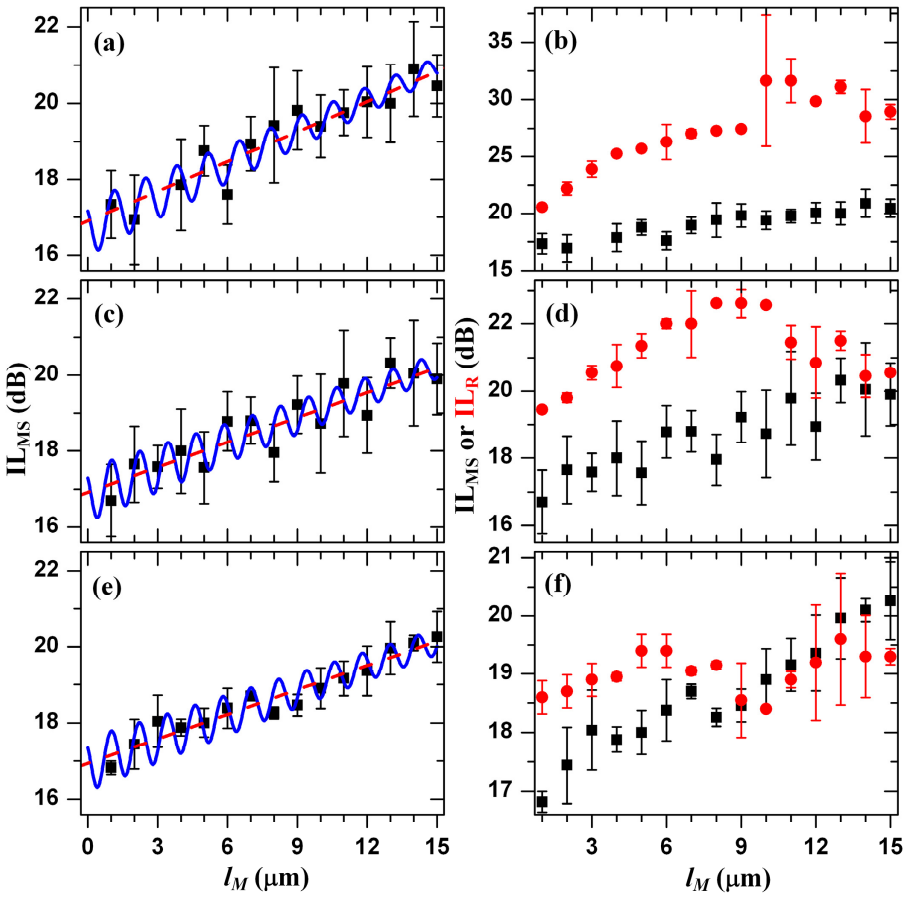

Fig. 3. Measured values of IL_{MS} vs. l_M for (a) w_S = ~160 nm, (c) w_S = ~190 nm, and (e) w_S = ~220 nm. They are represented by the square symbols with error bars. In these figures, the red dashed lines were obtained from the linear fitting, and the blue solid curves were obtained from the fitting based on Eq. (1). The measured values of IL_R are compared with those of IL_{MS} for (b) w_S = ~160 nm, (d) w_S = ~190 nm, and (f) w_S = ~220 nm. They are represented by the red circle symbols with error bars. The results in the figures were measured at λ = 1554 nm for TE polarization.

Table 1. Calculated values of $\overline{\beta}_M$ [a] and α_M [b] for the Different Values of ε_{Cu} at λ = 1554 nm

	w_S = ~160 nm		w_S = ~190 nm		w_S = ~220 nm	
ε_{Cu}	$\overline{\beta}_M$	α_M	$\overline{\beta}_M$	α_M	$\overline{\beta}_M$	α_M
$-79.6 - j10.9$ [17]	2.299	0.740	2.350	0.661	2.398	0.585
$-123 - j3.85$ [18]	2.243	0.130	2.300	0.115	2.353	0.101

[a] $\overline{\beta}_M = \beta_M / (2\pi / \lambda)$ [b] α_M is expressed in dB/μm.

In Fig. 3(b), 3(d), and 3(f), the measured values of IL_R are compared with those of IL_{MS}. The simulation based on the FEM shows that the reference waveguide starts to support a guided mode if w_S > 193 nm. If w_S = ~160 or ~190 nm, the reference waveguide does not support any guided mode, and so IL_R is larger than IL_{MS} for all the values of l_M. However, IL_R for w_S = ~220 nm become slightly smaller than IL_{MS} for w_S = ~220 nm if l_M > 10 μm. For a fixed value of l_M, as w_S decreases, IL_R increases; the increase of IL_R is much larger than the change of IL_{MS} depending on w_S. The comparison of IL_{MS} with IL_R shows that the existence

#173002 - $15.00 USD Received 20 Jul 2012; revised 4 Sep 2012; accepted 4 Sep 2012; published 10 Sep 2012

of the metal lines in the MISIM waveguide makes its loss quite different from that of the reference waveguide. Consequently, the comparison indirectly indicates that the MISIM waveguide supports a hybrid plasmonic mode.

Table 2. Resultant Values of the Fitting Parameters at λ = 1554 nm

w_S (nm)	L_t (dB)[a]	$\overline{\beta}_M$ [b]	α_M (dB/μm)	ϕ (rad)
~160	0.468	2.351	0.279	0
~190	0.451	2.287	0.224	0
~220	0.562	2.281	0.214	0

[a] $L_t = -10 \log T_t$ [b] $\overline{\beta}_M = \beta_M / (2\pi / \lambda)$.

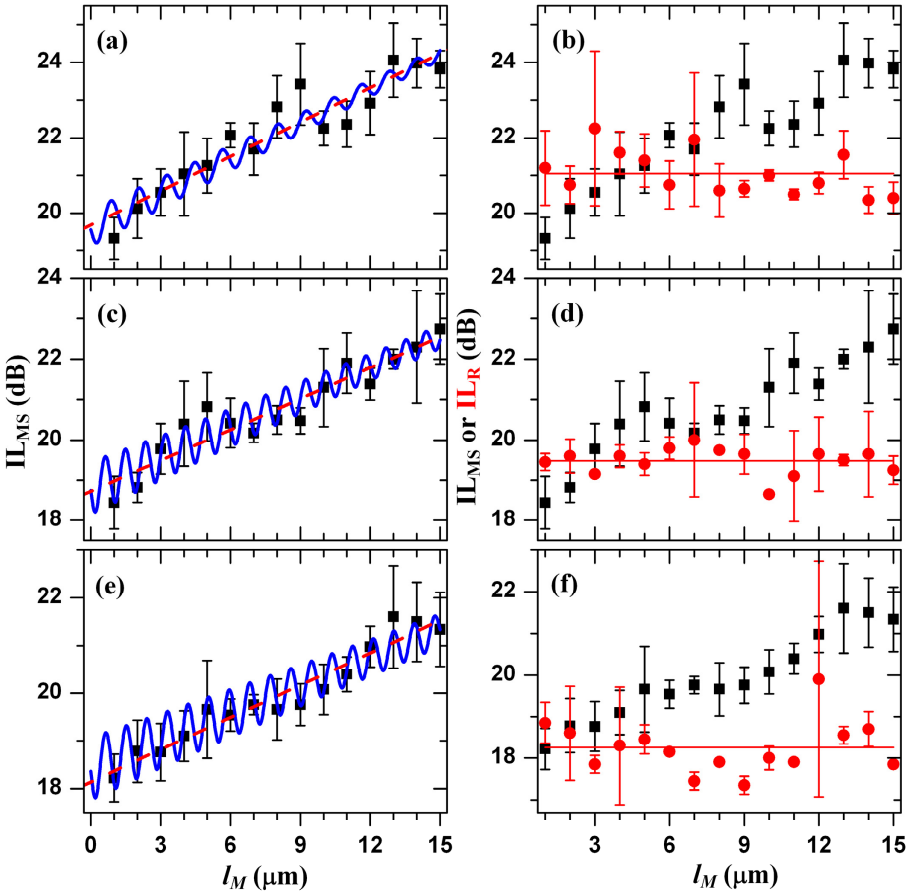

Fig. 4. Measured values of IL_{MS} vs. l_M for (a) w_S = ~160 nm, (c) w_S = ~190 nm, and (e) w_S = ~220 nm. The measured values of IL_R are compared with those of IL_{MS} for (b) w_S = ~160 nm, (d) w_S = ~190 nm, and (f) w_S = ~220 nm. The results in the figures were measured at λ = 1318 nm for TE polarization. The explanation of the symbols and lines in the figures are the same as in Fig. 3. Each red horizontal line corresponds to the average of the values of IL_R.

Figure 4(a), 4(c), and 4(e) show the values of IL_{MS} measured at λ = 1318 nm for w_S = ~160, ~190, and ~220 nm, respectively. In addition, the straight lines and the curves based on Eq. (1), which were fitted to the measured values, are shown together. The values of α_M from the slopes of the straight lines are 0.304, 0.255, and 0.226 dB/μm, respectively. The calculated values of β_M and α_M at λ = 1318 nm are summarized in Table 3. From the intercept of the fitted straight line for w_S = ~160 nm, L_t was extracted to be 0.48 ± 0.18 dB. In fitting the curves based on Eq. (1) to the measured values, α_{S2} and α_{S1} are 0.25 and 1.13 dB/mm,

#173002 - $15.00 USD Received 20 Jul 2012; revised 4 Sep 2012; accepted 4 Sep 2012; published 10 Sep 2012

respectively. Table 4 shows the values of the parameters related to this fitting. Although L_t should be positive, the values of L_t for w_S = ~190 and ~220 nm, which were obtained from both the linear fitting and the fitting based on Eq. (1), are negative due to measurement errors. The experimental values of L_t are smaller than the value obtained from FDTD simulation, which is 0.827 dB. The propagation loss of an SPP, which propagates along the interface between copper and dielectric, increases with λ decreasing, regardless of the models for ε_{Cu}. This plasmonic nature of the MISIM waveguide mode causes its propagation loss to increase as λ decreases. This is confirmed from a comparison of the values of α_M calculated with the model of ε_{Cu} in [17]. They increase by 0.156, 0.110, and 0.067 dB/μm, respectively, for w_S = ~160, ~190, and ~220 nm. However, such an increase due to the plasmonic nature depends on the values of ε_{Cu}, and it can be cancelled out due to photonic nature that the shorter the wavelength is, the larger portion of the power of the MISIM waveguide mode becomes confined to the Si line. This is confirmed from a comparison of the values of α_M calculated with the model of ε_{Cu} in [18]. They decrease by 0.02, 0.022, and 0.024 dB/μm, respectively, for w_S = ~160, ~190, and ~220 nm. In the cases of the experimental values of α_M, except for the value from the fitting based on Eq. (1) for w_S = ~220 nm, they increase. For example, those values obtained from the linear fitting increase by 0.042, 0.036, and 0.024 dB/μm, respectively, for w_S = ~160, ~190, and ~220 nm. These increases are three times smaller than the increases of the values calculated with the model of ε_{Cu} in [17].

Table 3. Calculated Values of $\overline{\beta}_M$ [a] and α_M [b] for the Different Values of ε_{Cu} at λ = 1318 nm

	w_S = ~160 nm		w_S = ~190 nm		w_S = ~220 nm	
ε_{Cu}	$\overline{\beta}_M$	α_M	$\overline{\beta}_M$	α_M	$\overline{\beta}_M$	α_M
–49.5 – *j*7.26 [17]	2.403	0.896	2.465	0.771	2.524	0.652
–88.0 – *j*2.35 [18]	2.323	0.110	2.397	0.093	2.467	0.077

[a] $\overline{\beta}_M = \beta_M / (2\pi / \lambda)$ [b] α_M is expressed in dB/μm.

Table 4. Resultant Values of the Fitting Parameters at λ = 1318 nm

w_S (nm)	L_t (dB)[a]	$\overline{\beta}_M$ [b]	α_M (dB/μm)	ϕ (rad)
~160	0.264	2.507	0.308	0
~190	*–0.129*	2.293	0.248	0.089
~220	*–0.324*	2.313	0.193	0

[a] $L_t = -10 \log T_t$ [b] $\overline{\beta}_M = \beta_M / (2\pi / \lambda)$

Interestingly, as shown in Fig. 4(b), 4(d), and 4(f), the values of IL_R seem to fluctuate around a constant value. (In each figure, the straight line represents the average of the values of IL_R.) Actually, FEM simulation shows that the reference waveguide starts to support a guided mode at λ = 1318 nm if w_S > 149 nm. Therefore, it is reasonable that IL_R does not change significantly when l_M changes only in the range of 1 to 15 μm. FDTD simulation shows that the excess loss of the symmetric coupler for the reference waveguide is 2.66, 1.33, and 0.45 dB, respectively for w_S = ~160, ~190, and ~220 nm. The increase of IL_R depending on w_S is related to the excess loss. Compared to IL_R, IL_{MS} tends to increase with l_M. Again this comparison clarifies that the MISIM waveguide mode is like a hybrid plasmonic mode.

3.2 Propagation characteristics for TM polarization

At λ = 1554 nm, IL_{MS} and IL_R for TM polarization were measured with respect to l_M. Figure 5 shows the relations of IL_{MS} and IL_R to l_M for the three values of w_S. For TE polarization, as shown in Fig. 3, IL_{MS} is smaller than IL_R except the case of w_S = ~220 nm for l_M > 10 μm. However, for TM polarization, IL_{MS} is much larger than IL_R, and IL_R tends to fluctuate around a constant value, which is the average of the values of IL_R in Fig. 5, like IL_R in Fig. 4. By means of FEM simulation, we can check that the reference waveguide starts to support a

#173002 - $15.00 USD Received 20 Jul 2012; revised 4 Sep 2012; accepted 4 Sep 2012; published 10 Sep 2012

guided mode for TM polarization if w_S > 159 nm. Thus the experimental result demonstrates that the metal lines of the MISIM waveguide disturb so seriously the guided mode of the reference waveguide. Actually, for TM polarization, no SPP-like wave can propagate along the interface between the metal line and the side insulator. Hence, the MISIM waveguide do not support any TM-polarized mode whose power is mainly confined to the Si line and the insulator around it. Consequently, the power of TM-polarized light incident from the 450-nm-wide Si photonic waveguide is significantly lost while it propagates in the MISIM waveguide via the symmetric coupler.

The overall propagation characteristics of the MISIM waveguide for both polarizations elucidate that it supports the TE-polarized mode (i.e. hybrid plasmonic mode) that possesses both the plasmonic nature and the photonic nature.

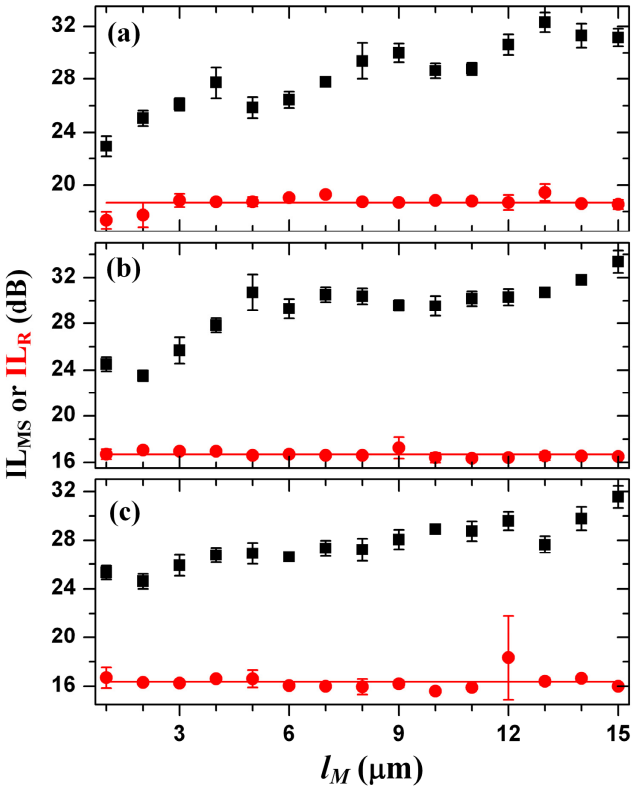

Fig. 5. Insertion losses at λ = 1554 nm for TM polarization. The measured values of IL_{MS} and IL_R are shown in (a), (b), and (c), respectively, for w_S = ~160 nm, ~190 nm, and ~220 nm. The values of IL_{MS} are represented by the square symbols with error bars, and those of IL_R are represented by the red circle symbols with error bars. Each red horizontal line corresponds to the average of the values of IL_R.

3.3 Excess losses due to the symmetric and asymmetric couplers

To check the dependence of the excess loss due to the symmetric coupler on its length l_t, at λ = 1554 nm, we measured IL_{MS} of the sets of the MISIM waveguides that have the symmetric couplers with l_t in the range of 0.3–1.0 μm. In addition, we measured IL_{MA} of the set of the MISIM waveguides whose w_S is ~190 nm and which have the asymmetric couplers with l_t in the range of 0.3–1.0 μm. The excess loss was extracted by using the relation $L_t = 0.5 \times [IL_{MS}$ (or IL_{MA}) – IL_{Si} (for l_{S1} = 4 mm) – α_M (in dB/μm) × l_M], where l_M = 1 μm. Figure 6(a) and 6(c) show the experimental values of L_t due to the symmetric couplers for w_S = ~160, ~190, ~220 nm. Figure 6(a) also shows the experimental values of L_t due to the asymmetric couplers for

#173002 - $15.00 USD Received 20 Jul 2012; revised 4 Sep 2012; accepted 4 Sep 2012; published 10 Sep 2012

w_S = ~190 nm. For the symmetric couplers, L_t is smaller than 0.5 dB for $l_t \geq 0.5$ μm, and it tends to increase slightly with l_t. As checked from Fig. 6(a), the asymmetric couplers cause larger excess losses than the symmetric couplers since the MISIM waveguide mode has a symmetric field distribution. Despite the larger excess losses, however, the former may be more useful than the latter when two closely placed MISIM waveguides are connected to two Si photonic waveguides. For comparison, we calculated L_t due to the symmetric and asymmetric couplers for w_S = ~190 nm, using FDTD simulation. The calculated values are shown in Fig. 6(b). Compared to the curves of L_t vs. l_t in Fig. 6(a), those in Fig. 6(b) have peaks, which are attributed to a sort of Fabry-Perot resonance of the symmetric and asymmetric couplers [14]. The experimental curves in Fig. 6(a) seem not to have such peaks since the widths of the Si lines of the realized couplers decrease to w_S more smoothly than expected from ideal linear tapering. Except for the peaks, the curves in Fig. 6(a) are somewhat similar to those in Fig. 6(b). A few negative values of L_t for w_S = ~220 nm arise due to measurement errors, and they do not mean gain.

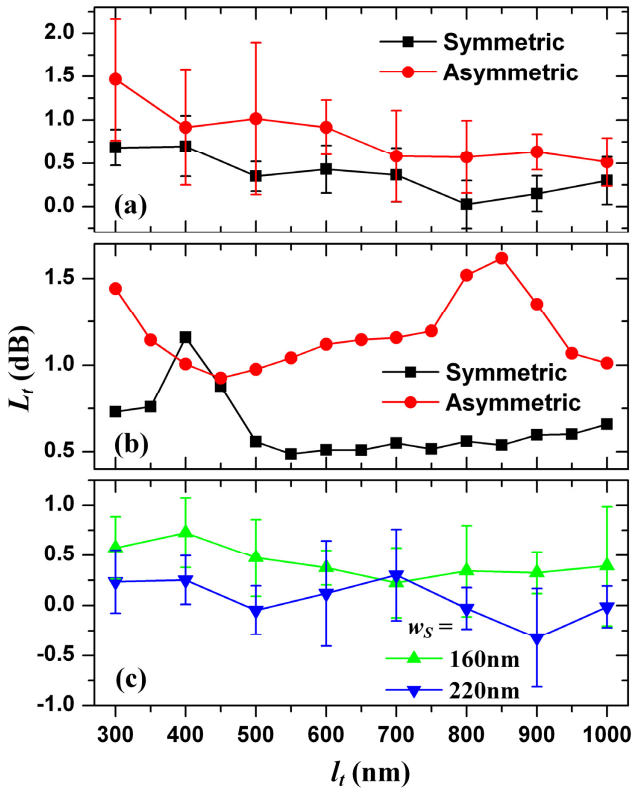

Fig. 6. (a) Measured values of L_t vs. l_t for w_S = ~190 nm. The black square (red circle) symbols with error bars represent the excess losses due to the symmetric (asymmetric) couplers. (b) Calculated values of L_t vs. l_t for w_S = ~190 nm. The black square (red circle) symbols represent the excess losses due to the symmetric (asymmetric) couplers. (c) Measured values of L_t vs. l_t for w_S = ~160 nm (the green triangle symbols with error bars) and ~220 nm (the blue inverted triangle symbols with error bars).

4. Removal of the insulator of the MISIM waveguide

As mentioned in Introduction, an important feature of the MISIM waveguide is that it can be used as a platform for functional nanoplasmonic devices. For this feature, as a first step, its insulator needs to be removed without damage to the metal lines. A simple way of removing the insulator is to use buffered oxide etchant (BOE). BOE is a mixture of hydrofluoric acid

#173002 - $15.00 USD Received 20 Jul 2012; revised 4 Sep 2012; accepted 4 Sep 2012; published 10 Sep 2012

(HF) and ammonium fluoride (NH_4F). However, BOE not only etches silicon oxide but also damages or corrodes copper. In order to prevent such corrosion, we mixed BOE with glycerol, which functions as a corrosion inhibitor [19, 20]. We used BOE (J. T. Baker) which consists of 34.9 weight percent NH_4F, 7.2 weight percent HF, and water. When BOE was mixed with glycerol (Junsei Chemical Co., Ltd.), the weight ratio of BOE to glycerol was 2:1.

Top and cross-sectional SEM images of the MISIM waveguide that was immersed in the mixture for 2 minutes are shown in Fig. 7(a) and 7(b), respectively. As shown in Fig. 7(b), a little part of SiO_x under the Cu and Si lines was etched away since immersion time was long. Figure 7(c) and 7(d) show the result obtained from immersion for 1 minute. As checked from Fig. 7(d), only the insulator between the Cu and Si lines are removed. The MSIM waveguides in Fig. 7 have w_S = ~190 nm, and their length is 5 μm. From this etching experiment, we successfully achieved 15-μm-long nanochannels with dimensions of about 30 nm × 250 nm, which may be filled with fluid or functional material.

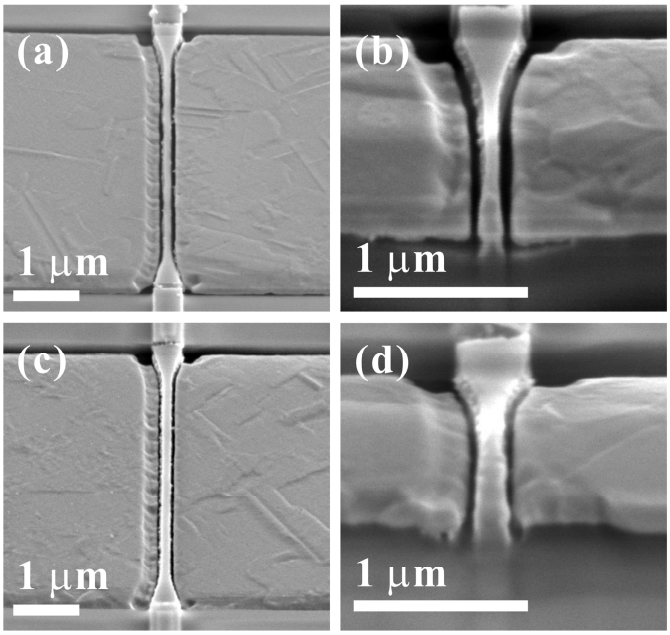

Fig. 7. (a) Top and (b) cross-sectional SEM images of the MISIM waveguides resulted from immersion in the mixture of BOE and glycerol for 2 minutes. (c) Top and (d) cross-sectional SEM images of the MISIM waveguides resulted from immersion for 1 minute.

5. Conclusions

We implemented the MISIM waveguide whose insulator is replaceable, using fully standard CMOS technology. The used fabrication process and the realized MISIM waveguides have been explained. The MISIM waveguides were made out of an 8-inch SOI wafer; the widths of their Si lines were ~160, ~190, or ~220 nm; the width of their insulator was 30 nm. We measured the propagation characteristics of the fabricated MISIM waveguides, and we have discussed the measurement results. For TE polarization, the propagation losses are between 0.2 and 0.3 dB/μm at λ = 1318 and 1554 nm. We have also shown that the symmetric and asymmetric couplers can be used to transfer efficiently optical power from the Si photonic waveguides to the MISIM waveguides. The excess losses due to the symmetric couplers are around 0.5 dB, which are smaller than those due to the asymmetric couplers. The propagation characteristics of the reference waveguides and those of the MISIM waveguides for TM polarization have indicated that the MISIM waveguide supports a hybrid plasmonic mode. Finally, we have successfully demonstrated that the insulator of the MISIM waveguide can be

#173002 - $15.00 USD Received 20 Jul 2012; revised 4 Sep 2012; accepted 4 Sep 2012; published 10 Sep 2012

removed to fabricate nanochannels without affecting the remaining MISIM structure. The MISIM waveguide whose insulator is removed may be a platform for functional nanoplasmonic devices. A future work may be filling the nanochannels with functional material like EO polymer. It may not be easy but possible to fill the narrow nanochannels since a 75-nm-wide nanochannel filled with EO polymer was reported previously [21].

Acknowledgments

This research was supported by Basic Science Program through the National Research Foundation of Korea (NRF) funded by the Ministry of Education, Science and Technology (2011-0025955).

#173002 - $15.00 USD Received 20 Jul 2012; revised 4 Sep 2012; accepted 4 Sep 2012; published 10 Sep 2012